Performance evaluation of linear variable valve actuation for a linear engine generator

Li, Mingqiang; Ngwaka, Ugochukwu; Wu, Dawei; Wang, Zhongcheng; Korbekandi, Ramin Moeini; Baker, Nick; Tsolakis, Athanasios

DOI:
10.1016/j.energy.2024.131361

Document Version
Publisher's PDF, also known as Version of record

Citation for published version (Harvard):
Li, M, Ngwaka, U, Wu, D, Wang, Z, Korbekandi, RM, Baker, N & Tsolakis, A 2024, 'Performance evaluation of linear variable valve actuation for a linear engine generator', *Energy*, vol. 298, 131361. https://doi.org/10.1016/j.energy.2024.131361

Energy 298 (2024) 131361

Contents lists available at ScienceDirect

Energy

journal homepage: www.elsevier.com/locate/energy

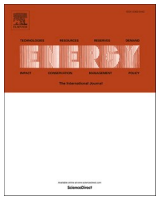

Performance evaluation of linear variable valve actuation for a linear engine generator

Mingqiang Li [a], Ugochukwu Ngwaka [a], Dawei Wu [a,*], Zhongcheng Wang [b], Ramin Moeini Korbekandi [c], Nick Baker [c], Athanasios Tsolakis [a]

[a] Department of Mechanical Engineering, University of Birmingham, B15 2TT, United Kingdom
[b] Merchant Marine College, Shanghai Maritime University, 201308, China
[c] School of Engineering, Newcastle University, NE1 7RU, United Kingdom

ARTICLE INFO

Handling editor: L Luo

Keywords:
Voice coil motor
Linear variable valve actuation
Linear engine generator
Energy analysis

ABSTRACT

The Joule cycle Linear Engine Generator (LEG) is a promising power generation technology with the potential to achieve zero carbon emissions. However, the LEG expander valve actuation system presents unique challenges due to its lack of a traditional crankshaft, the need for swift valve lift and reversal, and variable lift. This paper presents a Linear Variable Valve Actuation (LVVA) system for a LEG prototype. The LVVA system is powered by voice coil motors. Rigorous experimental investigations were conducted to analyze crucial performance factors, including energy consumption, force balance, energy flow distribution, and the relationship between valve lift duration and energy consumption. The results show that the LVVA system can achieve the desired valve lift and timing, as well as very small variations in LEG performance compared to the model using an ideal lift curve. The LVVA accounts for approximately 3.59 % of the LEG power output. The energy consumption of 1.607 J per valve stroke provides a slight advantage over traditional actuation systems. The obtained optimal lift curves were used to refine the LEG model. The influence of valve lift curves on LEG performance was evaluated which reveals rapid valve openings and relatively short duration contributing to improved LEG performance.

Abbreviations

EMF	Electromotive Force	F_{fp}	Friction force due to the pressure difference (N)
EVC	Exhaust valve closing	$F_{friction}$	Friction force (N)
EVO	Exhaust valve opening	F_{fv}	Viscous friction force (N)
HCCI	Homogeneous charge compression ignition	F_{mag}	Magnetic force (N)
IVC	Intake valve closing	F_p	Peak force (N)
IVO	Intake valve opening	i	Current (A)
LEG	Linear engine generator	k_f	Force constant (N/A)
LG	Linear generator	k_b	Back EMF constant (V/(m/s))
LVVA	Linear Variable Valve Actuation	L	Inductance (mH)
MAE	Mean absolute errors	$\dot{m}$	Mass flow rate (g/s)
VCM	Voice coil motor	p	Pressure (bar)
VVA	Variable Valve Actuation	p_{dif}	Pressure difference (bar)
Nomenclature		p_{up}	Upstream pressure (bar)
a_1	An empirical parameter for friction calculation (−)	P	Power (W)

(*continued on next column*)

(*continued*)

a_2	An empirical parameter for friction calculation (−)	P_a	Power consumption of the system (W)
A	Area (m^2)	P_c	Transient power of the coil (W)
A_l	Actual orifice area (m^2)	R	Resistance (Ohm)
C_f	The viscous damping coefficient (N • m/s)	R_e	rrrrEquivalent resistance (Ohm)
C_m	Mass flow parameter (−)	s	rrrrNormalized signal related to the valve position (−)
C_q	Flow coefficient (−)	t	rrrrTime (s)
D_B	Valve rod diameter(m)	t_l	rrrrLift time (s)
E	Energy (J)	t_r	rrrrResponse time (s)
E_a	Electromotive Force (V)	t_s	rrrrSpool valve action time (s)
f_d	Coulomb friction force (N)	T_0	rrrrPeriod time (s)
f_{dp}	Pressure friction coefficient (−)	T_{up}	rrrr Upstream temperature (K)
f_s	Stiction force (N)	U	rrrrVoltage (V)
F_a	Acceleration force (N)	w_p	rrrrContacting length (m)
F_{air}	Air force (N)	W_c	rrrrWeight of coil assembly (g)
F_c	Continuous force (N)	$\dot{x}$	rrrrVelocity (m/s)

(*continued on next page*)

* Corresponding author.
E-mail address: d.wu.1@bham.ac.uk (D. Wu).

https://doi.org/10.1016/j.energy.2024.131361
Received 13 October 2023; Received in revised form 29 March 2024; Accepted 17 April 2024
Available online 23 April 2024

(*continued*)

F_{dp}	Friction due to pressure difference (N)	$\ddot{x}$	rrrrAcceleration (m/s^2)
F_{fd}	Dry friction force (N)		

1. Introduction

The energy crisis and global climate change [1] pose significant engineering and scientific challenges in developing highly efficient energy conversion systems with low/zero environmental impact [2]. Concurrently, the push for decarbonization has accelerated research into these systems. Among these, a notably promising domain is the fuel cells fueled by hydrogen [3] or ammonia [4]. Notwithstanding their potential, several impediments hinder their deployment: high cost [5], limited lifespan [6], long time to start-up and operation with varying loads [7,8], challenges in thermal management and water heat balance in large-scale fuel cell systems [9,10], etc. Given these complex challenges, combustion-based systems and heat engines will remain central to energy conversion processes in power generation and propulsion systems for heavy vehicles and ships for the foreseeable future. While endeavors into refining conventional internal combustion engines and gas turbines are ongoing, including optimising the control methods to improve efficiency [11,12], recovering waste heat [13], and using green fuels [14], the development of new heat engines for heat recovery and low reactivity fuels will still be an important means of decarbonization. Among these emerging options, the Joule cycle Linear Engine Generator (LEG) has garnered significant attention over the past decades.

Various designs of the LEG have been concluded recently [15], and most designs of these reciprocating engines have eliminated the crankshaft to simplify the configuration and reduce frictional losses [16,17]. One example is the commercially available Mainspring's linear generator, which has a power level of 115 kW. It is an internal combustion type, capable of accommodating varying fuel quality and renewable options such as biogas, green ammonia, and green hydrogen. In the meanwhile, the Joule cycle LEG we have been developing [18] adopts an external combustion type, which can use green fuels such as hydrogen and ammonia; this configuration modification also enables LEG to use various energy sources, including solar energy and biomass, which contributes to the realization of low/net zero emissions [19,20]. Unlike earlier developed internal combustion LEGs, the stability of the Joule cycle LEGs does not depend on successful in-cylinder combustion, nor does it need to consider the challenges of coupling combustion and piston motion [21]. However, the valve timing and active intake and exhaust valve control are considered to significantly affect the performance and stability of the Joule cycle LEG [20]. Therefore, further investigation of the valve actuation system of the LEG is essential in the development of the Joule cycle LEG.

LEGs have re-emerged as a research hotspot since the 1990s [15]. They do not have a specialised valve actuation system, as their intake and exhaust mechanisms are based on those of conventional internal combustion engines. For instance, the Mainspring's linear generator uses scavenging ports to control the air in and exhaust out, while the other internal combustion type LEG uses the same principle. In 1998, Blarigan et al. [22] investigated a free-piston linear generator using Homogeneous Charge Compression Ignition (HCCI) to test different fuels. Scavenging ports were used for fuel/air mixture intake but the poppet valve was used for exhaust. In the same year, Clark et al. [23] developed a prototype of a two-stroke cycle linear engine alternator. Their design employed a pulsed solenoid fuel injector to control the intake of the fuel-air mixture, while scavenging ports were used for both intake and exhaust. Similarly, in 2015, Jia et al. [24,25] investigated the start-up and steady-state processes of a dual-piston free-piston engine generator, with scavenging ports serving as the intake and exhaust mechanisms. In 2020, Lu et al. [26] studied the synchronous motion control strategy and compression ratio control strategy of an opposed-piston free-piston engine generator. Their design also utilized scavenging ports for both intake and exhaust. It is noted that there is a lack of detailed research on valve actuation systems for LEG/traditional internal combustion free piston engines.

The Joule cycle LEG using external combustion was introduced in 2012 [27], featuring an external structural configuration that prevents the interaction between piston motion and combustion. However, the valve operation and timing significantly influence the force balance, the dynamic process of reciprocating movement, and ultimately affect the LEG's performance [20,27]. A prototype test rig with the dynamic and thermodynamic model was presented in 2018, and electro-pneumatic poppet valves were used for the expander intake and exhaust [28,29]. However, the electro-pneumatic valve actuation system has the drawback of a slow response time (t_r), which consists of the spool valve action time (t_s) required for the spool valve to open or close the ports by moving the piston in the cylinder, and the lift time (t_l) of the poppet valve. Standard pneumatic valves have a sliding spool or disk, and spool shift time typically ranges from 5 to 40 ms depending on the manufacturer (e.g., Parker Hannifin [30]). The spool shift time observed in the study [31] exceeded 12 ms. This could result in an excessively long response time; thus, a specially designed valve actuation system is necessary.

In search of a practical solution, Variable Valve Actuation (VVA) systems originally designed for conventional internal combustion engines were explored. Camshaft VVA exhibits limited flexibility as they are restricted by the position and configuration of the camshaft [32]. Furthermore, the intricate mechanical mechanism also presents a drawback, making camless VVA a more suitable choice for LEG. Camless-type VVA includes electro-pneumatic valves, electro-hydraulic valves, and electro-mechanical valves [33]. Fig. 1 (a) illustrates the configuration of the electro-hydraulic and electro-pneumatic valve actuation systems, and the primary difference between them is the type of working fluid used in the spool valve. Fig. 1 (b) displays the key components of the VCM valve actuation system, belonging to the electro-mechanical type. Table 1 outlines the advantages and disadvantages of various valve systems, along with typical case studies. For instance, the electro-hydraulic valve actuator was studied experimentally on a test bench. The results show that the electro-hydraulic actuator is superior in valve lift time and energy consumption, comparable to

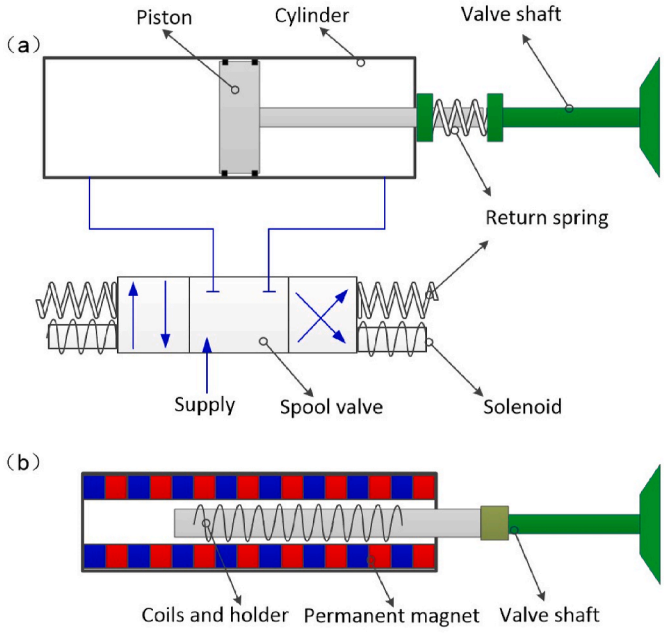

Fig. 1. Schematic configurations of the valve actuation systems: (a) electro-hydraulic valve system and electro-pneumatic valve system, (b) voice coil motor valve actuation system.

Table 1
Typical VVA systems used in the free-piston engine and the other engines.

Valve actuation type	Advantages	Disadvantages	Setup	Remark	Year
Electro-pneumatic	(1) Large force. (2) The viscosity of the working fluid is insensitive to temperature changes. (3) Air leakage does not impose pollution [42].	(1) Long spool response time in the pneumatic system. (2) Lower pressure force than hydraulic type. (3) Temperature swings need thermal management. (4) Difficult in achieving aimed lift profile and valve seating velocity. (5) Repeatability issues result from air compressibility. (6) Noise problems associated with exhaust, blockage, and hard valve seats [42].	Free-piston, rapid compression-expansion machine. Linear Joule Engine Generator. A Ford 4.6 L four-valve V8 engine Head.	No detailed information. No detailed information. The maximum valve lift height was 6 mm, with a 5 ms lift time.	1998 [22] 2018 [28,29] 2010 [35,36]
Electro-hydraulic	(1) Large force. (2) Variable lifts and good soft-land capability [43]. (3) Full flexibility of valve motion [42].	(1) Long spool response time in the hydraulic system. (2) Limited by the large viscosity at low temperatures [33]. (3) Operates only at low and medium engine speed. (4) High energy and cost requirements [42,43]	Hydraulic test bench.	3 ms lift time for 10 mm. 3.08 J and 1.99 J consumption for 8 mm and 1 mm strokes.	2013 [34]
VCM- driven pneumatic	(1) Quick spool response with quick valve port opening and closing. (2) Large force.	Drawbacks as the other pneumatic system.	VCM force test bench.	With a lift of 0.5 mm, the pneumatic spool response time could be about 0.3 ms. No response time information about this valve system.	2013 [44], 2013 [37]
VCM	(1) Simple structure. (2) Easy to realize small-scale, high-frequency, and high-precision reciprocating control [45]. (3) Rigidity system. (4) Fast response speed. (5) Operates quietly. (6) High linearity, and no cogging force nor pulsation [46].	(1) Sensitive to external disturbances and load changes. (2) Mechanical resonance. (3) Low thrust density [45].	MATLAB/Simulink model. Simple experimental setup. Test bench. Spring-assisted test bench Model and test bench	With a 10 mm stroke, the lift time is about 5 ms, and the seating velocity is about 0.02 m/s. With an 8 mm stroke, lift time is 3.8 ms and a seating velocity of 0.05 m/s. Lift time of 6.9 ms from 0.4 mm to 7.6 mm stroke. Precise movement with a steady-state error within 0.02 mm. Generated a starting force of 574.92 N at 11 A. Stroke up to 8 mm, and the time needed is 104 ms. With 3 A current, the force reaches 549.2 N. The starting force can be as high as 574.92 N at current 13.66 A. The transition time is 4.8–6.9 ms. When the stroke is 8 mm, the steady-state error is within ±0.02 mm.	2005 [38] 2012 [39] 2021 [40] 2022 [47] 2022 [41]

that of a conventional internal combustion engine valve consuming 1.5 J–4.0 J of energy per stroke [34]. This performance is attributed to the low moving mass and the strong force generated by the hydraulic system. Pneumatic valves were tested with different strokes and various pneumatic pressure in an engine head, with a promising lift time of 3 ms–5 ms for lifts ranging between 4 mm and 6 mm [35,36]. However, it is important to note that neither the hydraulic nor the pneumatic valve tests mention the spool valve action time (t_s), which is a key factor in the rapid reversal of the valve.

Considering the disadvantages of the electro-hydraulic valve system and electro-pneumatic valve system, electro-mechanical actuators, without spool valve action time (t_s), gain attention due to their fast response times (t_r), the simple configuration and management. Especially for the VCM type, the flat force and travel curve also contribute to its suitability for these applications. In 2014, Wu et al. [37] used VCMs in the electro-hydraulic servo valve to drive the spool valve. A peak thrust of 140 N was detected at a current of about 6 A to open the spool valve ports. However, there is no report of the response time of this VCM-directly driven pneumatic spool. Moreover, there are some attempts to use the VCM to actuate the poppet valve directly. In 2005, Khandaker et al. [38] built a VCM-type VVA simulation model with a seating velocity of 0.02 m/s and a 5 ms lift time without experimental validation. In 2012, Liu et al. [39] designed an electro-magnetic valve actuator powered by VCM. A dynamic model and a control method were developed, and the experimental results achieved a lift time of 3.8 ms and a seating velocity of 0.05 m/s, proving the effectiveness of the proposed method. In 2021. Fan et al. [40] developed a VCM-type electro-magnetic linear actuator for internal combustion engines and tested the dynamic performance without loads on a test bench. The actuator achieved a lift time of 6.9 ms from 0.4 mm to 7.6 mm, precise movement with a steady-state error within 0.02 mm, and generated a starting force of 574.92 N at 11 A. In 2022, Fan et al. [41] designed a composited electromagnetic valve actuator to enhance the force of the VCM and reduce energy consumption at different motion mode. A paek force of 574.92 N can be achieved when the VCM and a moving iron electromagnetic linear actuator wor together; and a passive holding force of 229.25 N can be achieved without additional current. The test outcomes above, along with the comparison of VVA performance in lift, time, and energy consumption shown in Table 3, together highlight the suitability of the VCM-type valve actuation system for the Joule cycle LEG.

In summary, the Joule cycle LEG incorporates an external burner, providing flexibility in fuel selection and enabling the utilisation of

Table 2
Specifications of the voice coil motors.

Parameters	Unit	LVVA-intake VCM	LVVA-exhaust VCM
Quantity	[−]	2	1
DC resistance, R_0	[Ω]	5.5	6.3
Peak force constant, k_f	[N/A]	41.2	26.6
Back EMF constant, k_b	[V/m/s]	41.2	26.6
Inductance, L	[mH]	4.3	1.6
Peak force, F_p	[N]	262	140
Continuous force, F_c	[N]	115	42.2
Weight of coil assembly, W_c	[g]	275	80

green fuels like hydrogen and ammonia. This configuration also allows for sustainable energy sources such as solar, geothermal, and nuclear energy, thereby achieving low/zero emissions. However, this external burner configuration presents valve design challenges, such as variable stroke, variable time, and quick reversal time of the valves in the LEG [20]. Valve actuation system plays a key role in LEG performance, but the current research is mainly focused on performance and control of the system, and there is a lack of in-depth research on force balance, dynamic characteristics and energy consumption. Only a few studies have attempted to compensate for the low power density and energy consumption of VCM type VVA [41,47]. Moreover, the impact of valves on LEG performance, including the analysis of experimental lift curves, has yet to be comprehensively explored within the LEG model's framework.

To bridge these research gaps, a Linear Variable Valve Actuation (LVVA) system was developed, comprising poppet valves, VCMs, drives, encoders, and supports, forming a fully variable valve actuation system. This paper aims to design and evaluate the performance of the LVVA for a lab-scale LEG [48]. Experimental tests were conducted based on the actuation system test rig, and the results were analyzed in detail about the system's dynamics characteristics and energy consumption. The relationship between energy consumption and valve timing per stroke was examined to improve understanding of LVVA performance. Furthermore, the actual lift curves were used to refine the LEG model and assess the effect of the valve lift curves on the LEG performance.

2. Methodology

The methodology flow chart is depicted in Fig. 2, which is used to explore the LVVA performance and its impact on the LEG performance. In the following sections of methodology, it starts with the introduction of the LEG model which has been validated in the previous papers. Based on the desired valve performance set by the LEG model, the LVVA experimental rig is developed, at the meantime, the LVVA model is constructed and to be validated with the experimental data. LVVA dynamic characteristics and energy analysis will be conducted, while the LVVA performance from the experiments will be further incorporated into the LEG model for enhanced performance predictions.

2.1. The validated LEG model

The LEG model is built with Simcenter AMESim, which features a set of variable time-step numerical integration solvers, capable of autonomously determining the best integration method for the system. The LEG model has been comprehensively validated in references [18,49,50]. The LEG model is a multidisciplinary model that integrates the thermal dynamic model, friction model, and Linear Generator (LG) model. The validation was based on a combined approach using both experimental data and simulation, with specific focuses on key parameters such as displacement, velocity, and acceleration in engine dynamics. Fig. 3

Table 3
Comparison of engines' valve actuation system performance.

Engine type	Unit	Joule cycle LEG	Yanmar diesel engine NFD 13 K [61]	Ford Mondeo engine, 2.0 L V4 Duratec [62]	Cooperative Fuels Research engine [63]	SI gasoline engine [64]
Engine speed	[RPM]	[−]	3000[a]	3500	1500	3600
Frequency	[Hz]	10	50	58.3	25	60
VVA type	[−]	VCM	Electro-magnetic	Electro-hydraulic	Electro-magnetic	Hydraulic
Intake valve lift	[mm]	5.5	8.5	8	8	5.5
Intake valve lift duration	[ms]	20.12	25.5–27.2	>8.5[b]	10–27.8	~10.42
Intake valve Energy consumption per cycle	[J]	1.4	3.14–3.78	3.08	2.2–6.95	8.17[c]
Exhaust valve lift	[mm]	6.24				5.5
Exhaust valve lift duration	[ms]	40.08				~9.72
Exhaust valve Energy consumption per cycle	[J]	0.207				

[a] Based on the valve actuator frequency.
[b] The sum of the opening and closing time is 8.5 ms, without the dwell time at max lift.
[c] Total energy consumption of one intake valve and one exhaust valve.

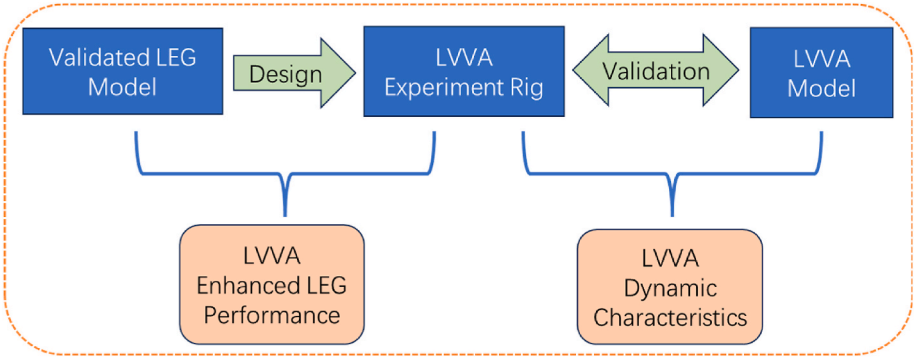

Fig. 2. Flow chart of methodology.

depicts the agreement of the experiment and the simulation results for piston displacement, which has the maximum deviation of 7.28 %. The LG serves as a critical component in force balance of LEG, which was simulated using Simcenter Magnet. The validation has undergone rigorous testing, ensuring a high level of model accuracy. The consistency between experiments and simulations on key parameters of LG was achieved, such as induced no-load electromotive force (EMF), shown in Fig. 4.

2.2. The valve model of the LEG

As for the poppet valve model in the LEG expander, the mass flow rate is expressed in Equation (1) [51,52]:

$$\dot{m} = A_l \bullet C_q \bullet C_m \bullet \frac{p_{up}}{\sqrt{T_{up}}} \tag{1}$$

where C_q is the flow coefficient and is used to include extra losses due to local friction and loss of kinetic energy, C_m is the mass flow parameter, p_{up} and T_{up} are the upstream pressure and temperature, respectively. A_l is the actual orifice area, which is expressed as:

$$A_l = s \bullet A_r \tag{2}$$

where s is a normalised signal to represent the valve lift position. It is an ideal pulse signal in the LEG model, and the experimental lift curves were converted to replace it. A_r is the real orifice area.

The valve model in the LEG model is used for estimating the key parameters in the duty cycles of LVVA. After the LVVA experiment, a detailed LVVA model will be constructed for further analysis.

2.3. Design specifications

The LVVA comprises the exhaust valve actuation part (LVVA-exhaust) and the intake valve actuation part (LVVA-intake). These two would work together to achieve the working fluids in and out of the LEG expander. Based on the LEG simulation requirements, as introduced below, a large magnetic force and short response time are required to ensure the necessary reciprocating movement frequency.

Figs. 5 and 6 depict the pressure variations on both sides of the intake valves and exhaust valve at a frequency of 10 Hz. In Fig. 5, the pressure preceding the intake valve (solid black line) shows slight fluctuations because of the compressor's valve opening and closing. In contrast, the expander cylinder's pressure (black dotted line) undergoes significant changes as the working fluid expands during the process since the intake

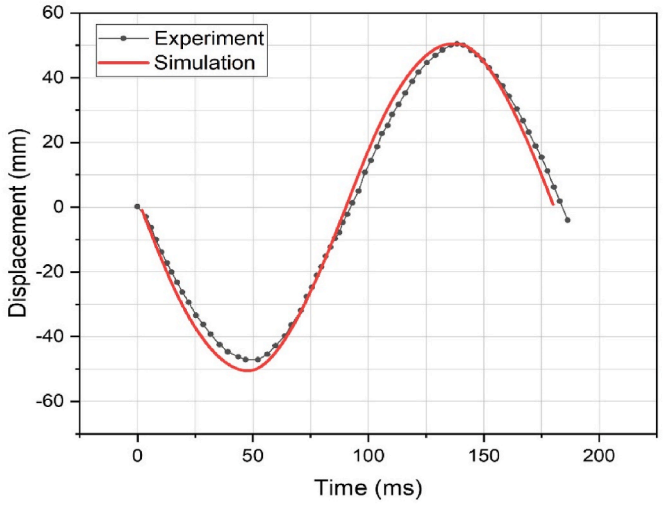

Fig. 3. Comparison of experimental and simulation results of the LEG displacement [49].

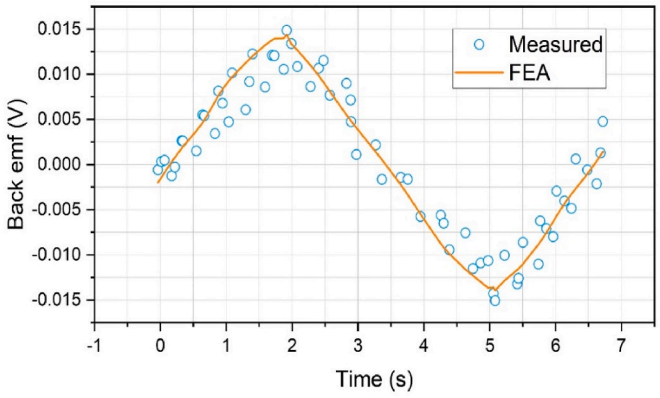

Fig. 4. Comparison of experimental and simulation results of the no-load back EMF of the LG [50].

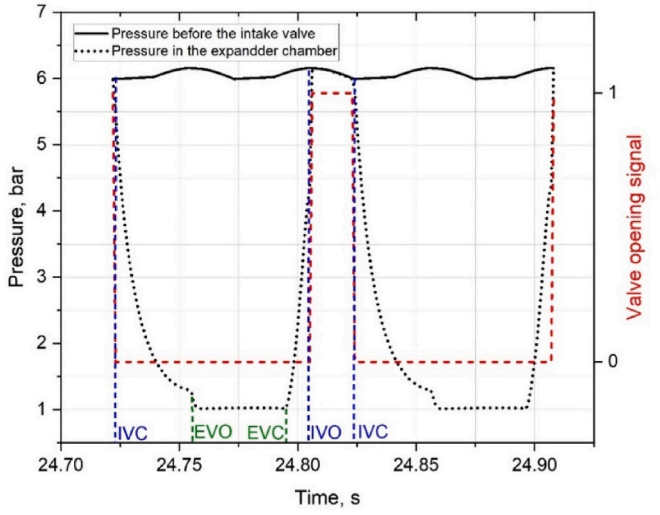

Fig. 5. The pressure changes on both sides of the intake valve.

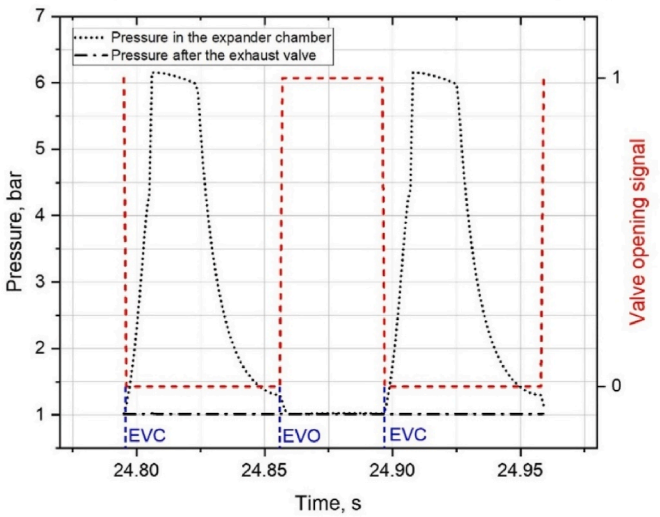

Fig. 6. The pressure changes on both sides of the exhaust valve.

valve closing (IVC). The pressure after the exhaust valve (black dash-dot line) represents the ambient pressure, 1 bar. The red dotted lines illustrate the ideal pulse signals of valve opening and closing.

In Fig. 5, the air in the expander is compressed and works as a gas spring since the exhaust valve closing (EVC). At the intake valve opening (IVO), the intake valves open with a pressure difference of approximately 1.77 bar. While in Fig. 6, the exhaust valve opens at exhaust valve opening time (EVO) with a pressure difference of about 0.29 bar. These pressure differences decrease rapidly to almost zero after the valves open. According to simulations, the gas forces on the intake and exhaust valves are approximately 134.57 N and 14.24 N, respectively, but they only last for a short time. The opening time of the exhaust valve is about 40 ms, and the opening time of the intake valve is about 20 ms.

Therefore, VCMs were selected, and their specifications are summarized in Table 2. The force constant changes along with the position are illustrated in Fig. 7. Therefore, the design details of the LVVA are presented: in Fig. 8, a single exhaust valve (in green) is guided and supported by a bronze guide placed in the exhaust head chamber; two intake valves (in blue) are in the intake expander head chamber and are supported by two bronze guides; also, bronze/graphite bearings are used for support and bearing, and PTFE U-seals are implemented to prevent leakage from the expander head chamber.

2.4. LVVA test rig and experimental procedure

The experiments were conducted on part of the LEG prototype, shown in Fig. 9. The total moving mass of the LVVA-exhaust is 0.224 kg, and it is 0.837 kg for the LVVA-intake. A Compact Veratus Series encoder was used to detect the real-time position of the valves; a 60 V, 15 A, BK1902BDC power supply was used for powering; an ACJ-055-18 was used to drive the VCMs. The high-pressure gas required for the actuation system experiment rig was provided by the Clarke Boxbr 14/200 air compressor, while the DVP LC 106 pump was used in the LVVA-exhaust test to create an evacuated environment within the expander head chamber. EWCTV-312 M pressure transducers, with a full scale reading of 10 V ± 300 mV, were used to detect the pressure changes in the expander head chambers, while the NI compact RIO 9056 and the module of NI 9222 were used for pressure monitoring.

The compressor supplied the compressed air of 2.77 bar to ensure that the pressure difference between the intake valves' two sides was the same as the LEG model, and a vacuum pump kept the pressure lower than the environment pressure to represent the 0.29 bar pressure difference. The voice coil motors were launched, and the poppet valves' positions, the current, and the voltage of the power supplies were recorded.

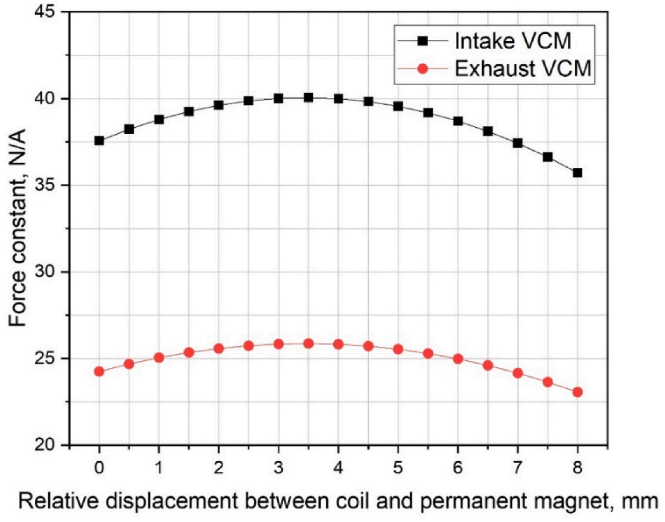

Fig. 7. Force constant changes with the relative displacement between the coil and permanent magnet.

3. LVVA system modeling

3.1. Actuation system circuit

A DC power supply powers the voice coil motors of the actuation system, while the ACJ-055-18 motor drive adjusts the voltage, current, and power for the voice coil motor via the PID control based on position feedback from the encoder. When current flows through the circuit, there will be a magnetic force propelling the coil assembly forward or backward, and there will be Electromotive Force (EMF, E_a) generation resulting from the movement of the current. The EMF of the voice coil motor could be expressed as [53]:

$$E_a = k_b \bullet \dot{x} \tag{3}$$

where k_b means the back EMF constant, with a unit of V/(m/s), and $\dot{x}$ is the velocity of the coil assembly, with a unit of m/s.

The field-effect transistors and sense resistors have some resistance in the drive, typically 0.075–0.4 Ω, according to the manufacturer Copley Controls. The equivalent circuit of the voice coil motor and the drive could be described by the equivalent circuit, as shown in Fig. 10. The drive is described as a power supply with a typical resistance of R_0, while the coil is described by resistance, inductance, and EMF. Therefore, the equivalent circuit in Fig. 10 (b) illustrates the circuit of the LVVA-exhaust [54]. Two voice coil motors work in parallel in the LVVA-intake; the equivalent circuit is presented in Fig. 10 (a).

Based on Kirchhoff's voltage law, the voltage balance of the circuit for the LVVA-exhaust could be expressed as [43,53]:

$$U = E_{a1} + i \bullet R_1 + i \bullet R_0 + L_1 \bullet \frac{di}{dt} \tag{4}$$

$L_1 \bullet \frac{di_1}{dt}$ in Equation (4) indicates that inductance voltage exists when the changing current passes through the coil. The voltage of the intake valve system is expressed in Equation (5):

$$U = \left(E_{a1} + i_1 \bullet R_1 + L_1 \bullet \frac{di_1}{dt}\right) + i \bullet R_0 \tag{5}$$

where U means the voltage from the drive, and i is the current of the equivalent circuit. The subscripts 1 and 2 in the circuit mean the first voice coil motor and the second voice coil motor separately, R_1 and R_2 are the resistances of the parallel coils, R_0 is the equivalent resistance of the drive, L_1 and L_2 are the voice coil inductances.

3.2. Actuation system dynamic model

The force balance of the moving coil assembly, which consists of the voice coil, rod, coupling, and valves, is expressed in Equation (6):

$$F_a = F_{mag} + F_{air} + F_{friction} \tag{6}$$

$$F_{mag} = k_f \bullet i \tag{7}$$

$$F_{air} = p_{dif} \bullet A \tag{8}$$

where F_{mag} is the magnetic force and could be calculated as the product of the current, i and force constant, k_f [43]. F_{air} is the air force results from the pressure difference changes with time, p_{dif}, and the valve force area, A. $F_{friction}$ is the friction force, and F_a is the acceleration force.

The friction force consists of two parts. The first is friction, F_{fp}, due to the pressure difference between the expander head chamber and the ambient, and it originates from the U-Cup seals and the rods; the second is the dry friction, F_{fd}, of the valves and the bearings/seal. They could be expressed as [49,55]:

$$F_{friction} = F_{fp} + F_{fd} \tag{9}$$

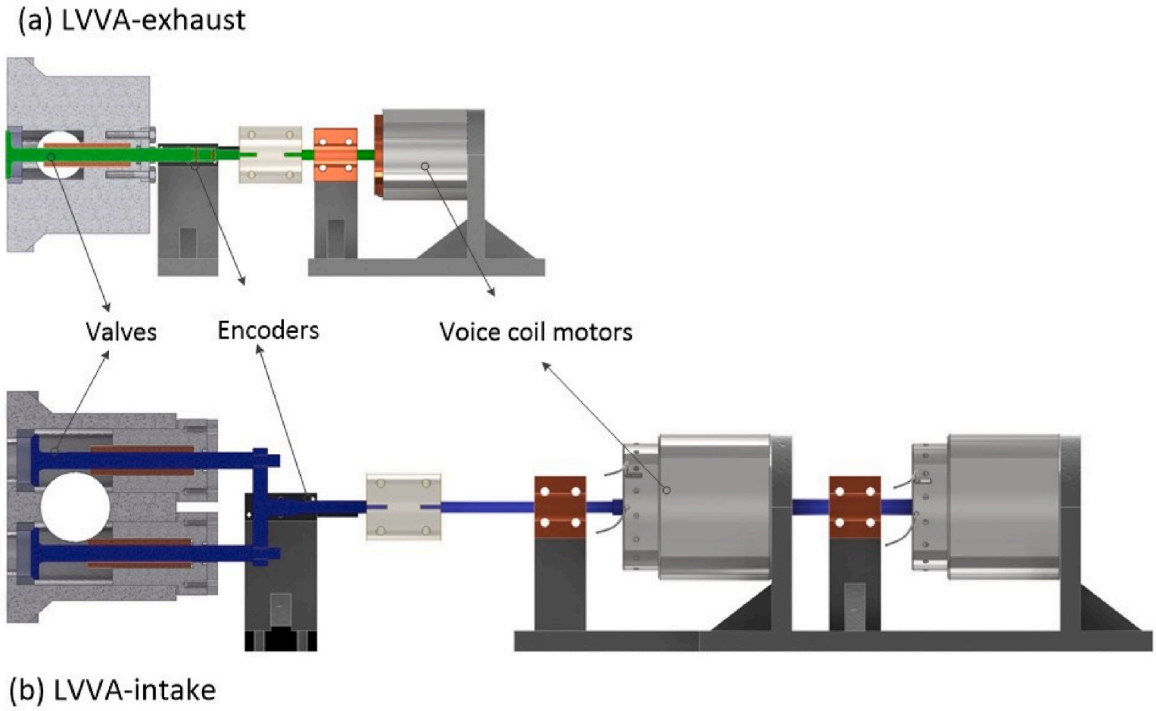

Fig. 8. Schematic diagram of (a) LVVA-exhaust and (b) LVVA-intake.

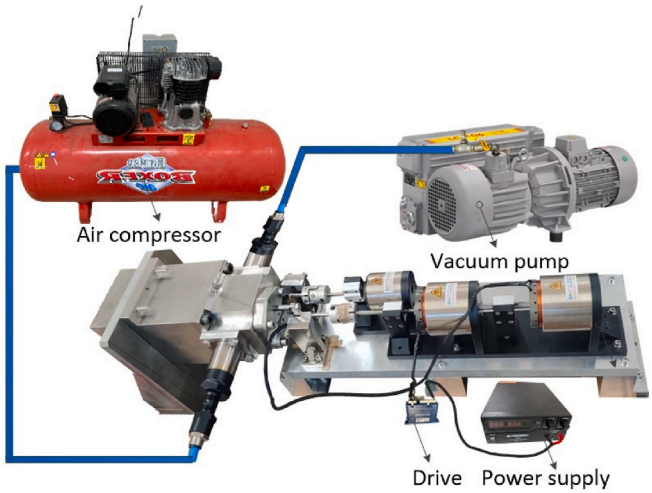

Fig. 9. Experiment rig of the LVVA.

$$F_{fp} = f_{dp} \bullet \pi \bullet p_{dif} \bullet D_B \bullet w_p \tag{10}$$

$$F_{fd} = \left[f_d + (f_s - f_d) \bullet \exp\left(-\frac{a_1 \bullet |\dot{x}|}{|\ddot{x}| + a_2} \right) \right] \bullet \text{sign}(\dot{x}) \tag{11}$$

where the f_{dp} is the pressure friction coefficient, p_{dif} is the pressure difference between the expander head chamber and the ambient, and D_B is the valve rod diameter, w_p is the contacting length of the valve rod and the bearing/seal. f_d is the Coulomb friction force, f_s is the Stiction force, a_1 and a_2 are empirical parameters, and $\ddot{x}$ is the acceleration. The friction coefficient of stainless steel and bronze graphite was considered 0.1, while the coefficient (f_{dp}) of stainless steel and PTFE was 0.05 [56]. Dry friction parameters were: $f_d = 0.25$, $f_s = 0.3$, $a_1 = 12$, and $a_2 = 0.1$ [55].

3.3. Energy flow and distribution

Energy flow throughout the system is evaluated using the equivalent circuit. The power from the power supply would flow in several directions, including the resistance load power ($i^2 \bullet R_e$), transient inductance power of the coil (P_c), the power required to overcome air resistance, the power required to overcome friction, and the power required to convert into kinetic energy, as expressed in Equation (12):

$$P_a = U \bullet i = i^2 \bullet R_e + P_c + (F_{air} + F_{friction} + F_a) \bullet \dot{x} \tag{12}$$

where P_a is the power consumption of the system, and R_e is the equivalent resistance, which contains the resistance of the coils and the drive.

During the operation, a coil inductor can store and release energy with the changes in the current. When the current flowing through the inductor increases and di/dt becomes greater than zero, the instantaneous power in the coil becomes positive ($P_c > 0$), indicating that the electrical energy is being stored in the coil. Conversely, when the current through the coil inductor decreases the instantaneous power becomes negative ($P_c < 0$), implying that the inductor is releasing energy back to the circuit.

Additionally, there is energy transfer between kinetic and electric power during acceleration and deceleration [57]. Notably, during deceleration, the EMF acts differently than during acceleration: it works together with the drive to provide the voltage required for the actual resistance and converts the kinetic energy of the mover into electricity.

It should be noted that the valve seats at a very low velocity, leading to virtually no collision. As a result, the energy loss from this impact is considered negligible. Besides, there's a minimal change in the current when the valve seats. This suggests that the voice coil motor's coil primarily releases its inductance stored energy during the deceleration phase. Consequently, we infer that throughout a full lift cycle, the energy flow direction excludes the release of energy stored in the coil post-seating. Therefore, the energy conversion during one cycle, as described in Fig. 11, includes the electrical loss in the drive, the motor electrical loss, the friction loss, and the load (gas force loss).

In this case, during one period time of T_0, the energy (E) could be

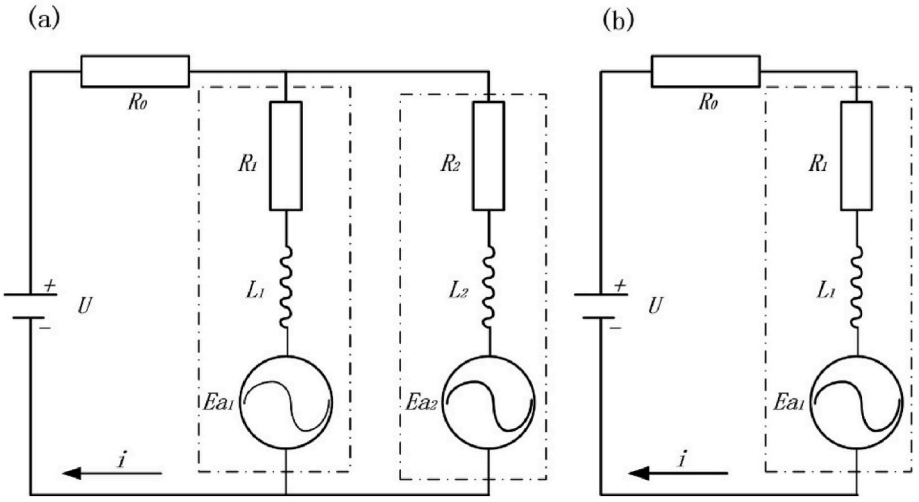

Fig. 10. Equivalent circuits of the (a) LVVA-intake and (b) LVVA-exhaust.

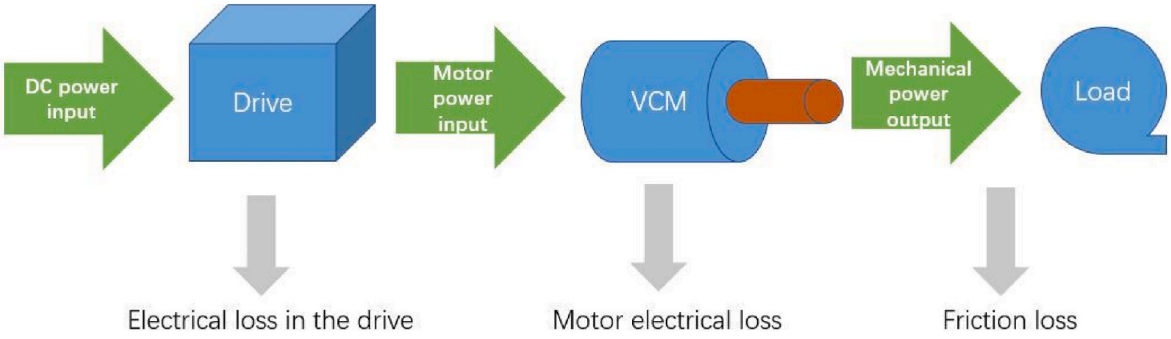

Fig. 11. LVVA power consumption distribution and direction.

expressed by:

$$E = \int_0^{T_0} \left(i_t^2 \bullet R_e\right) dt + \int_0^{T_0} \left(F_{friction} \bullet \left(\int_0^t (\ddot{x} \bullet t) dt\right)\right) dt + \int_0^{T_0} \left(F_{air} \bullet \left(\int_0^t (\ddot{x} \bullet t) dt\right)\right) dt \quad (13)$$

where i_t means the current changes with time, and the first part is the energy consumption in the equivalent resistance, including the coils and equivalent resistance in the drive; the second part is the friction loss, and it is the product of friction and velocity over time; the third part describes the air force loss.

4. Results and discussion

4.1. Experimental lift curves

Fig. 12 describes the valve motion profiles of the experiment results. The lift for the intake valves is about 5.5 mm, and it is about 6.24 mm for the exhaust valves, with about 0.02 mm position error and 0.02 mm/s seating velocity, which is better than the reported level [39]. For the intake valves, the lift time is approximately 9.12 ms, and the duration is about 20.12 ms. The exhaust valve lift time is around 12.88 ms, with a duration of 40.08 ms. Furthermore, the VCM's response time can be as short as approximately 3 ms, indicating the response time it takes to react following a trigger signal.

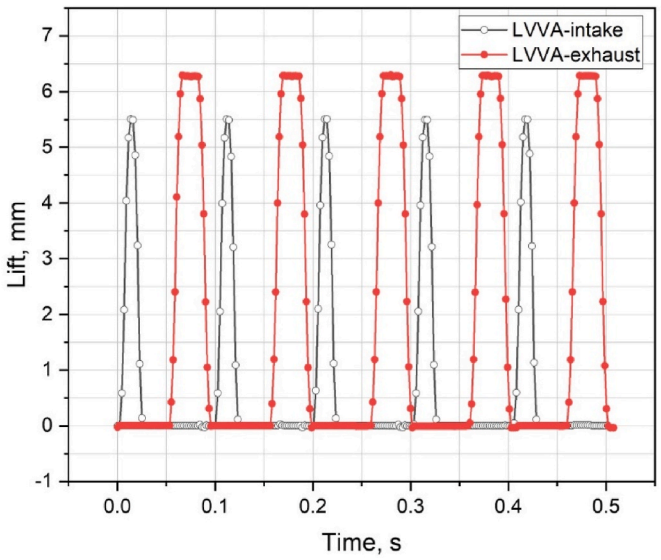

Fig. 12. Valve lift profiles of the LVVA-intake and LVVA-exhaust.

4.2. Performance and dynamic analysis of LVVA

The detailed movement profiles of the experiment results of the LVVA-intake and LVVA-exhaust are shown in Fig. 13 (a) and (b), respectively. Both figures depict the changes in valve lift and velocity during one cycle of engine operation, with a period of about 100 ms. The

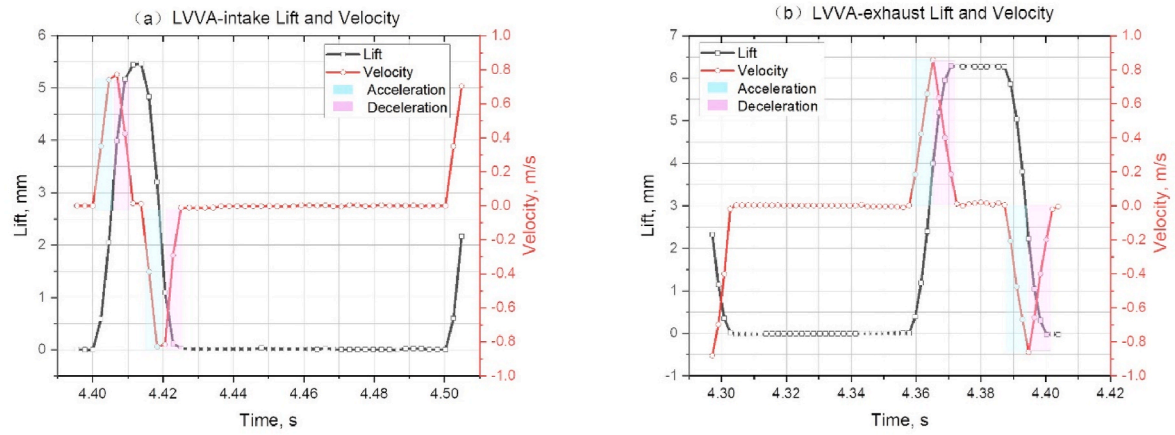

Fig. 13. The lift and velocity of the valves: (a) LVVA-intake and (b) LVVA-exhaust.

velocity of the exhaust valve could reach 0.86 m/s in (a), while the peak velocity of the intake valves was about 0.77 m/s in (b). The lower peak velocity of the LVVA-intake was due to its shorter lift time and lower acceleration. The trajectory of both valves can be divided into six distinct processes: the acceleration (reseda domain) and deceleration (light pink domain) during the forward movement, maintaining in the valve fully open position, the acceleration (reseda domain) and deceleration (light pink domain) during the backward movement, and finally settling in the fully closed position [58].

Fig. 14 (a) and (b) show similar changes in current and voltage, respectively, during the LVVA-intake and LVVA-exhaust operation. Both figures provide insight into the energy conversion details of the systems. Before launching the valves, there is a stage of starting (light brown domain), during which the magnetic force needs to counteract the air force and friction. This requires a large current to provide the necessary magnetic force. At the same time, the emerging current would result in an EMF generated in the coil; therefore, the voltage from the drive during this period is the sum of the EMF and the voltage needed for the current generation [59]. During the acceleration process, both the mover's kinetic energy and the EMF increase. During the deceleration process, the EMF generated sometimes could have the same direction as the applied voltage, based on Lenz's Law [57]. This EMF will combine with the voltage from the VCM drive to create the required voltage, the same phenomenon could also be seen in Ref. [60]. This results in different voltage magnitudes from the VCM drive for the acceleration and deceleration processes. The backward process exhibits similarities with the forward process, except for the impact of gas force. Both the LVVA-exhaust and LVVA-intake experience comparable changes in current and voltage, but there are differences in their peak values due to limitations imposed by the specifications of the VCM and the system's robustness. In Fig. 14 (a), the LVVA-intake demonstrates peak current and voltage values of approximately 6.16 A and 39.60 V, respectively; while in Fig. 14 (b), the LVVA-exhaust reaches peak current and voltage levels of approximately 1.11 A and 27.11 V, respectively. It is worth noting that there is still a current of about 0.1 A for the LVVA-intake and 0.04 A for the LVVA-exhaust existing for a short time to control the seating speed and avoid severe collision, which was also observed in Ref. [59].

Force analysis was conducted to validate the forces and the force balance of the movers. The magnetic force was derived from the actual position data, current values, and force constant; and the force balance was used to estimate the sum of the experimental air force ($F_{air,e}$) and friction force ($F_{friction,e}$). Moreover, the air compressor provided continuous compressed air, and the changes in the pressure differences between the two sides of the valves were estimated based on the simulation results of the LEG model, enabling theoretical estimation of the gas force ($F_{air,c}$). Various types of friction were considered theoretically ($F_{friction,c}$), including friction caused by pressure differences between expander head chambers and ambient air, friction between the stainless-steel valve rod and the bronze carbon guide/bearing, and friction between the stainless-steel valve rod and the PTFE U-seal.

The study compared theoretical and experimental forces, including air and friction forces. The forces and position profiles of the LVVA-intake and LVVA-exhaust are shown in Figs. 15 and 16, respectively. The short black dashed line represents the sum of the experimental forces, including friction and air forces ($F_{friction,e} + F_{air,e}$). At the same

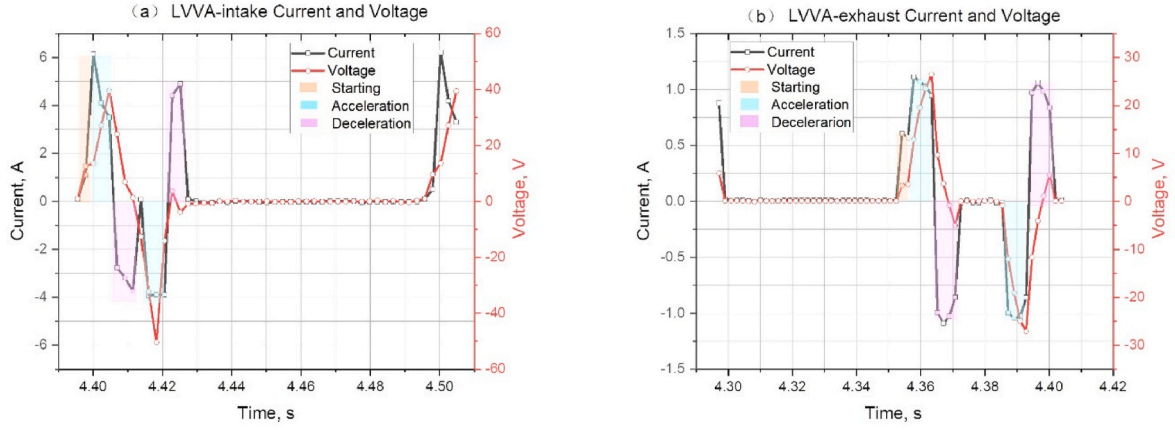

Fig. 14. Current and voltage from the VCM drive: (a) LVVA-intake and (b) LVVA-exhaust.

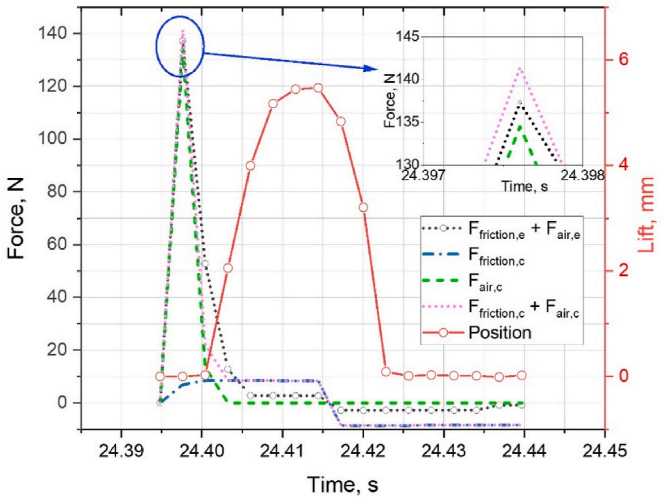

Fig. 15. Comparison of the forces between the experimental and theoretical calculation in LVVA-intake.

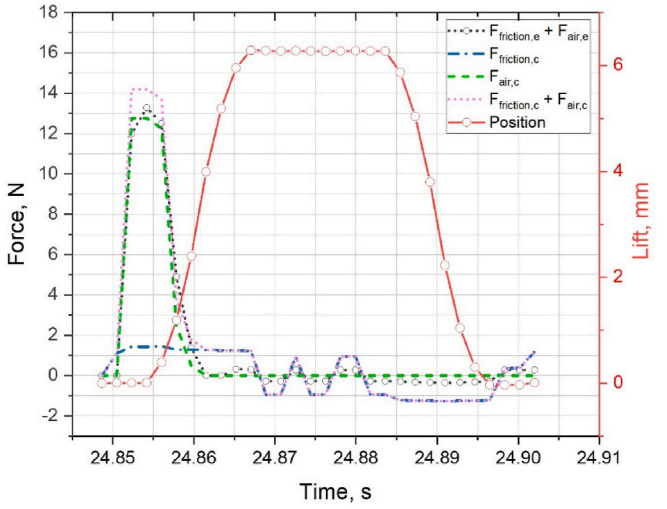

Fig. 16. Comparison of the forces between the experimental and theoretical calculation in LVVA-exhaust.

time, the other dash and short dot lines represent the friction and air forces ($F_{friction,c}$ and $F_{air,c}$) and the sum of both, which were calculated theoretically. At the start of the lift, the air force ($F_{air,c}$) was significant and decreased as the lift increased. The friction force ($F_{friction,c}$) was low and changed direction with lift velocity. The experimental peak force ($F_{friction,e} + F_{air,e}$) in LVVA-intake was about 137.31 N, which is 2.9 % smaller than the theoretically calculated. On the other hand, those on the LVVA-exhaust were smaller, and the experimental peak load force (13.29 N) was about 6.41 % smaller than the theoretical of 14.20 N. The sampling rate and the difference between the pressure variations within the chamber and the simulated results may cause these peak value errors. Based on these results, the force balance model of the valves is considered appropriate and reflects the dynamic characteristics of the system.

4.3. Energy flow and energy consumption

With the validation of the force balance model, Equation (12) was used to evaluate the energy consumption per cycle of the LVVA-intake and LVVA-exhaust. The total power required for the LEG's valve actuation, which includes two sets of both LVVA-intake and LVVA-exhaust, amounts to approximately 32.14 W. The LVVA-exhaust consumed approximately 0.207 J, with a range of 0.199–0.211 J, while the LVVA-intake required approximately 1.40 J per cycle, with a range of 1.35–1.45 J. All the variation range are below 3.9 %, and they arise from the resolution of the pressure transducer and the pressure variations from compressor and pipes. These mean energy consumptions are comparable to the 1.5 J–4.0 J valve actuation consumption of the traditional internal combustion engine, as per reference [34].

The LVVA-intake and LVVA-exhaust have the same energy flow directions, as shown in Fig. 17. Most of the energy is lost as heat through resistive losses, with motor electrical losses accounting for 84.66 % and 92.29 % for the LVVA-intake and LVVA-exhaust, respectively. The difference in proportions was primarily due to differences in current magnitudes, shown in Fig. 14. The friction loss is higher in the LVVA-intake than the LVVA-exhaust because of moving mass and gas pressure differences between the systems. Both systems experience low levels of gas force loss, below 2.2 %, because the pressure difference only affected the beginning of the launch.

As for the performance of LVVA, it was contrasted in Table 3 with the other valve actuation systems. For LVVA's valve stroke, its performance in multiple valve drive systems is moderate, which is related to the size of the valve port. Regarding the valve's lift duration, due to insufficient data, we can only compare based on duration continuity, finding that LVVA's performance is average. Notably, when it comes to energy consumption, LVVA stands out with a significant advantage. The hydraulic valve drive system tends to consume a substantial amount of energy related to the hydraulic system. In the meanwhile, the electromagnetic type, given its inherent electromagnetic system characteristics, greater acceleration, and extended valve stroke, also exhibits higher energy consumption.

4.4. Further investigation of LVVA performance and energy consumption

The study investigated the performance of LVVA-intake and LVVA-exhaust at different strokes and the lift curves are presented in Figs. 18 and 19, respectively. Experimental results showed that at an air pressure difference of 1.77 bar, the LVVA-intake achieved strokes of 3.94 mm, 5.50 mm, and 6.77 mm, with corresponding energy consumptions of 0.613 J, 1.400 J, and 1.889 J. As the stroke increased, the lift time also increased [43], while limitations in power supply and motor drive current restrict the maximum achievable stroke. The LVVA-exhaust achieved strokes of 4.03 mm, 5.50 mm, 6.24 mm, and 8.05 mm, with energy consumptions of 0.102 J, 0.182 J, 0.207 J, and 0.383 J, respectively. Moreover, the increasing lift times in LVVA-intake

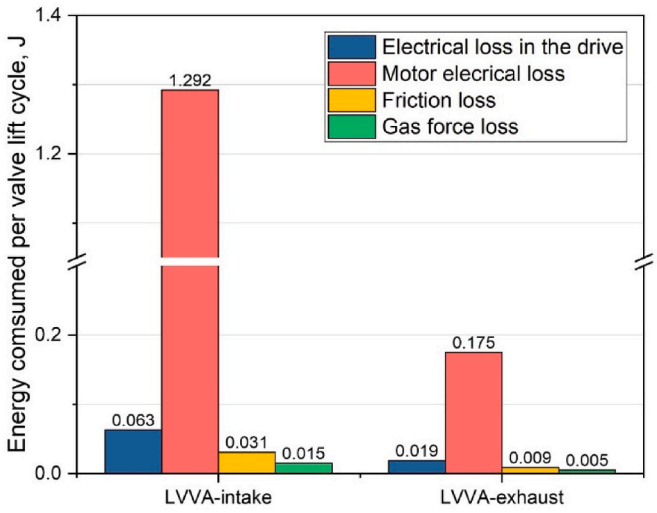

Fig. 17. Comparison of energy flow distribution of LVVA.

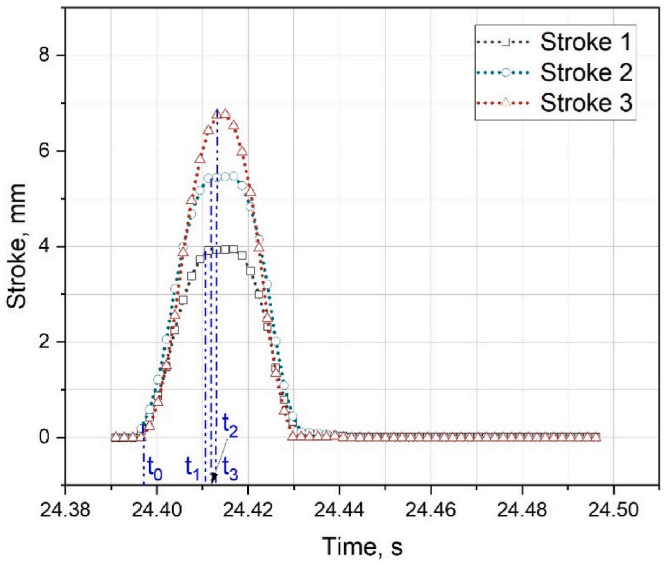

Fig. 18. Different stroke curves for the LVVA-intake.

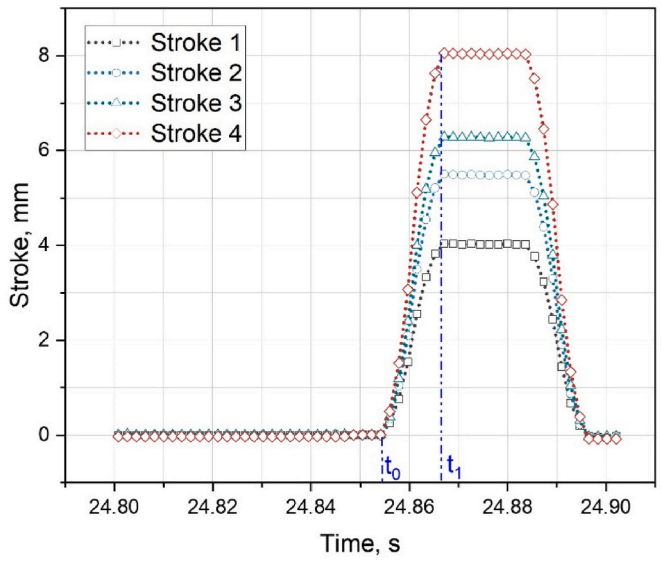

Fig. 19. Different stroke curves for the LVVA-exhaust.

shows it could not achieve better performance while lifting time t1 in the LVVA-exhaust shows the potential of achieving longer strokes. This is due to the difference in the moving mass and the magnetic force.

Different pressure differences were tested under the conditions of a fixed stroke and fixed acceleration. The LVVA-intake consumed 1.172 J and 1.400 J at 0 bar and 1.77 bar pressure differences, respectively. While the LVVA-exhaust required 0.191 J and 0.207 J at pressure differences of 0 and 0.29 bar. Although the proportions of gas forces were relatively low, the pressure difference significantly affected energy consumption. Overcoming the required air force demanded a larger current, leading to increased electrical losses in the motor and drive system, resulting in higher energy consumption.

Studying the impact of stroke and differential pressure on energy consumption enhances our understanding of the performance of LVVA-intake and LVVA-exhaust systems. It also demonstrates the way to optimize the system in the aspects of decreasing energy consumption and the response time: reducing the mover's mass, thereby reducing the required current magnitude for a given acceleration demand [43].

Fig. 20 compares the lift time and the energy consumption per stroke

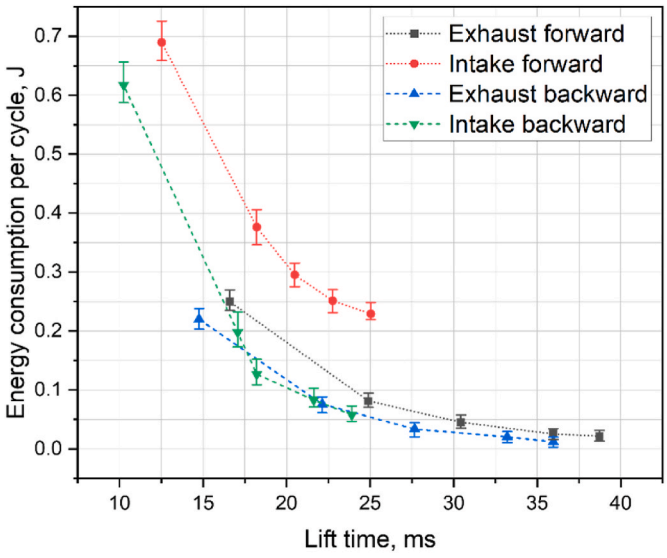

Fig. 20. Energy consumption characteristics of LVVA.

for both LVVA-intake and LVVA-exhaust. When stroke is restricted to 6.24 mm, the forward and backward LVVA-exhaust processes consumes less than 0.25 J each. The larger the energy consumption, the shorter the lift time would be [59,65]. Due to the gas force, the forward process requires a longer lift time and more energy than the backward process. The backward process has the shortest lift time of about 15 ms and the longest lift time of about 36.5 ms. Similar trends are observed for the LVVA-intake with a 5.5 mm stroke, albeit with higher energy requirements and shorter completion times. The maximum energy required is approximately 0.69 J for the forward process, with a short lift time of 12.5 ms, while it needed 0.62 J and 10.5 ms to complete the backward process. The minimum energy required for the LVVA-intake forward and backward processes were 0.23 J and 0.06 J, respectively. The difference in consumption between the LVVA-intake and LVVA-exhaust results from the difference in the gas loads, moving mass, and VCM specifications; however, the gas loads mainly contributed to the difference in the forward and backward processes for it would affect the current effectively.

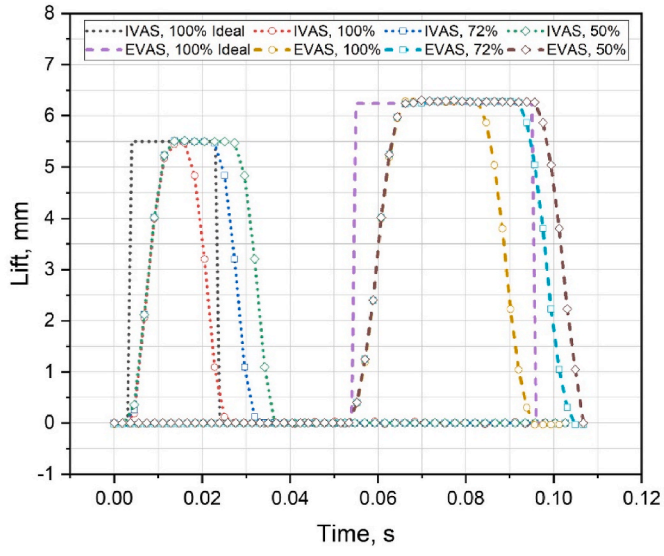

Fig. 21. Comparison of the valve lift curves.

4.5. Valve performance effect on the LEG

Fig. 21 compares valve lift curves, both ideal pulse curves and experimental lift curves. These experimental lift curves correspond to 100 %, 72 %, and 50 % loads in the LEG model to evaluate the effect of the experimental curves on LEG performance. The 100 % load case using the experimental curves, which were analyzed in the previous section, is closest to the ideal pulse valve lift curve and achieves the closest LEG performance using the ideal curve. It is characterized by a short lift time, and the other experimental curves have almost the same shape of the lift curve as the 100 % load case, but with a longer full-open duration.

Fig. 22 depicts the correlation between piston velocity and displacement using various lift curves. Using the Ideal Pulse Curves (Ideal), the LEG model exhibits the highest peak velocity, followed by the 100 % load experimental case. This exhibits lower velocity when the pistons move away from the operation top and bottom dead centre (a and b) but higher values as they approach a and b. Meanwhile, with the smallest loads, case 50 % using experimental curves has the shortest stroke and the lowest peak velocity, resulting in the lowest engine efficiency and power output.

The performance of the LEG model with the Ideal Pulse Curve (Ideal) and the refined LEG model, which incorporates the experiment lift curves, are compared in Table 4. The 100 % load experimental lift curve achieves nearly the same LEG performance compared with the ideal situation. Engine efficiency of the 100 % load case decreases by 1.09 %. Nevertheless, the mechanical power output increases by 0.13 % compared to the ideal case, which generates 897.07 W.

The increase in mechanical power output can be attributed to reduced friction loss and changes in magnetic force. During the leaving of points a and b in Fig. 22, there are smaller friction forces in the 100 % load case compared to the Ideal case, due to the smaller pressures in the cylinders as shown in Fig. 24, and the lower velocity in Fig. 22. Additionally, the higher pressure at point B in Fig. 24 and the slightly longer duration of the valve opening lead to a slightly increased mean mass flow rate, which further contributes to the power increase [65]. However, it should be noted that a comparison of the experimental cases indicates that a longer intake valve opening time can result in a noticeable decrease in both power output and engine efficiency, which was also presented in Ref. [20].

Figs. 23 and 24 depict the changes in mass and pressure within the expander chamber individually. These figures provide a detailed comparison between the Ideal case and experimental curve cases. At Point A,

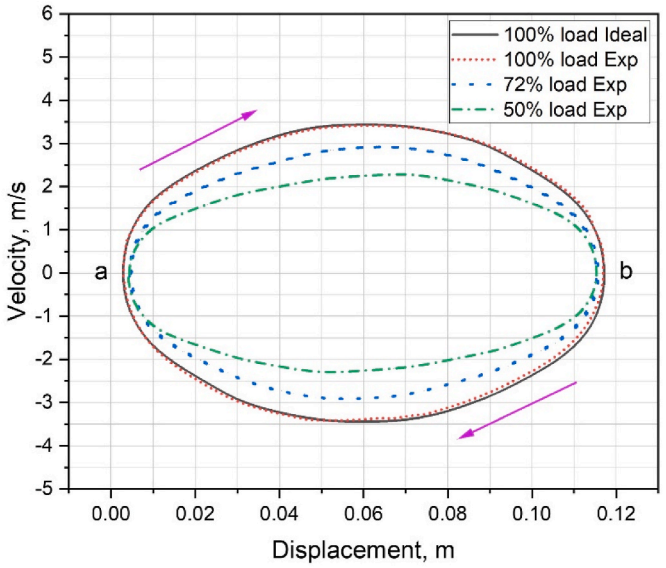

Fig. 22. Comparison of the velocity changes along with the displacement.

Table 4
Performance comparison of the LEG employing ideal pulse curve and experimental lift curves.

Cases	Unit	Ideal	100 % load	72 % load	50 % load
Intake valve opening time	[ms]	20.00	20.12	29.64	41.04
Exhaust valve opening time	[ms]	40.00	40.08	49.68	58.88
Stroke	[mm]	114.27	113.99	111.38	110.96
Peak velocity	[m/s]	3.44	3.41	2.92	2.28
Mean mass flow rate	[g/s]	8.87	8.88	8.47	7.81
Engine efficiency	[%]	25.17	24.89	22.46	15.69
Mechanical power output	[W]	895.94	897.07	650.71	447.98

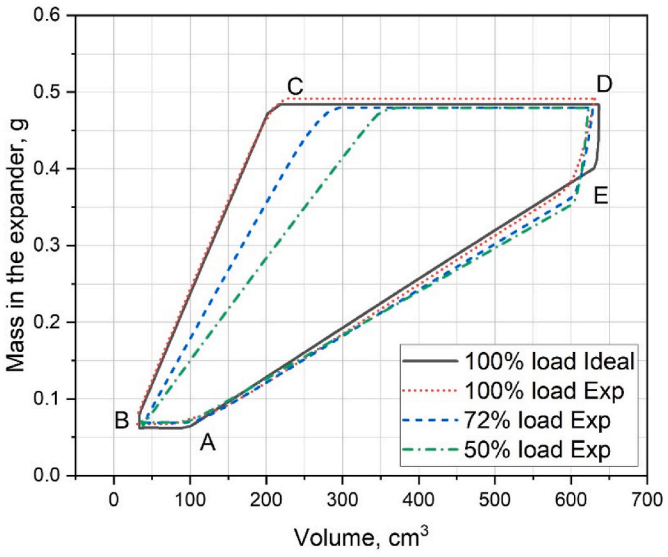

Fig. 23. The mass changes along with the expander chamber volume.

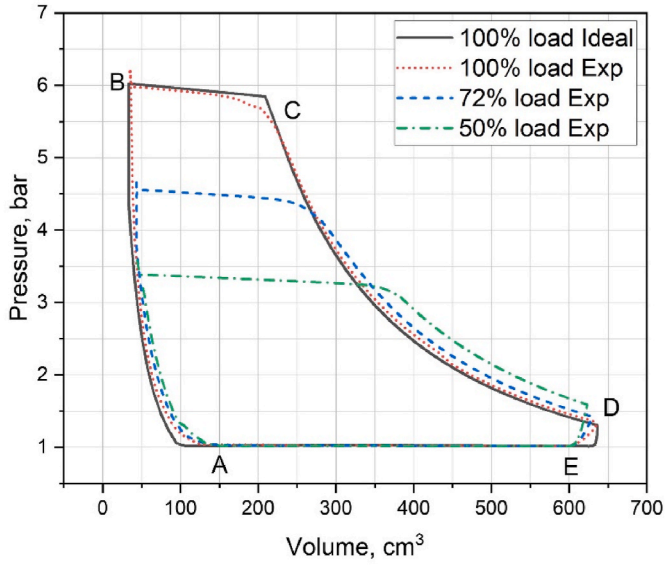

Fig. 24. The pressure changes along with the expander chamber volume.

the exhaust valve closes, initiating the generation of the air spring. The discrepancy between the Ideal Pulse Curve (Ideal) and experimental curve (100 % load) results in variations in air spring generation. It should be noted that there is a spike at position B, caused by the final pressure of the air spring exceeding the compressor pressure. This phenomenon aligns with the experimental results [28]. Point C corresponds to the closure of the intake valves, and the experimental lift curves yield slightly lower pressures compared to the Ideal case. Points D and E represent the gradual opening of the exhaust valve, and the differences in curve shapes and pressures account for the variations in the pressure decrease during this period. The chamber's mass is also affected by the stroke difference, which reflects the changes in mass within the chamber. The differences in curve shapes similarly lead to variations in the mass change processes, mirroring those observed in the pressure changes.

After refining the model using experimental lift curves, Fig. 25 illustrates the relationship between valve opening time, engine efficiency, power output, and the reciprocating frequency of the piston system. It is evident that a slower frequency corresponds to longer valve opening times but adversely affects the LEG performance of the engine, as reported in Refs. [18,20]. Furthermore, the lower frequency leads to a shorter stroke and smaller peak pressure, as well as a reduced mass flow rate, ultimately resulting in lower engine efficiency and decreased power output [18].

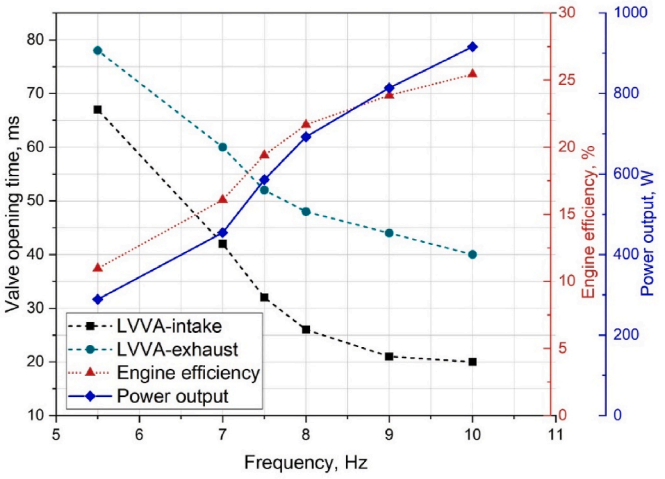

Fig. 25. The relationship between the frequency and the valve opening times, and the LEG performance.

5. Conclusion

A Linear Variable Valve Actuation (LVVA) system is designed, prototyped, tested, and used for the perfromation prediction of a Joule cycle LEG. Compared with camshaft VVA, LVVA eliminates the need for multiple cam profiles and intricate control mechanisms. Apart from its advantages in efficiency, flexibility, large driving force, and energy saving, the key findings are:

(1) The rapid response time of LVVA benefits from the removal of the spool valve action time within hydraulic and pneumatic systems. It achieves a quick response time of 3 ms and a 0.02 mm/s seating velocity at aim lift.
(2) The LVVA uses about 0.207 J (exhaust valve) and 1.40 J (intake valve) during one cycle when the frequency of the LEG is 10 Hz. Gas force leads to larger energy consumption, in turn, shorter lift time for both intake and exhaust systems.
(3) The majority of energy loss of the LVVA system dissipates in the form of heat due to motor coil resistance, with electrical losses accounting for 84.66 %–92.29 % of the total loss. LVVA-intake experiences higher friction loss due to its larger moving mass and higher pressure difference.
(4) The LVVA can achieve the desired stroke with acceptable lift times in a real-life system. The experimental valve profile of LVVA achieves slight engine power increase (0.13 %) and minor decrease (1.09 %) in engine efficiency compared to the LEG model using the ideal valve model.

Future work will entail modifying the LVVA and applying it to the LEG prototype as well as other engines. Initial experimental and numerical analyses have underscored the need to optimize the LVVA system's structure and reduce the mass of its moving unit. This reduction in mass can lead to faster valve response times and significant energy savings.

CRediT authorship contribution statement

Mingqiang Li: Formal analysis, Investigation, Methodology, Writing – original draft, Writing – review & editing. **Ugochukwu Ngwaka:** Investigation, Methodology. **Dawei Wu:** Conceptualization, Funding acquisition, Investigation, Methodology, Project administration, Supervision, Writing – review & editing. **Zhongcheng Wang:** Conceptualization, Methodology. **Ramin Moeini Korbekandi:** Conceptualization, Methodology. **Nick Baker:** Conceptualization, Methodology. **Athanasios Tsolakis:** Funding acquisition, Supervision.

Declaration of competing interest

The authors affirm that they do not have any known financial interests or personal relationships that may have influenced the work reported in this paper.

Data availability

Data will be made available on request.

Acknowledgement

This work was supported by EPSRC (Engineering and Physical Sciences Research Council, United Kingdom) (Grant numbers: EP/S00193X/2, EP/Y024605/1). The first author would also like to thank the support from China Scholarship Council for the Stipend Scholarship awarded.

References

[1] Olabi AG, Abdelkareem MA. Renewable energy and climate change. Renew Sustain Energy Rev 2022/04/01/2022;158:112111. https://doi.org/10.1016/j.rser.2022.112111.
[2] Olabi AG, et al. Assessment of the pre-combustion carbon capture contribution into sustainable development goals SDGs using novel indicators. Renew Sustain Energy Rev 2022/01/01/2022;153:111710. https://doi.org/10.1016/j.rser.2021.111710.
[3] Abe JO, Popoola A, Ajenifuja E, Popoola OM. Hydrogen energy, economy and storage: review and recommendation. Int J Hydrogen Energy 2019;44(29):15072–86.
[4] Machaj K, et al. Ammonia as a potential marine fuel: a review. Energy Strategy Rev 2022/11/01/2022;44:100926. https://doi.org/10.1016/j.esr.2022.100926.
[5] Korberg AD, Brynolf S, Grahn M, Skov IR. Techno-economic assessment of advanced fuels and propulsion systems in future fossil-free ships. Renew Sustain Energy Rev 2021/05/01/2021;142:110861. https://doi.org/10.1016/j.rser.2021.110861.
[6] Zhang Y, et al. A techno-economic analysis of ammonia-fuelled powertrain systems for rail freight. Transport Res Transport Environ 2023;119:103739. https://doi.org/10.1016/j.trd.2023.103739.
[7] Abdelkareem MA, Elsaid K, Wilberforce T, Kamil M, Sayed ET, Olabi A. Environmental aspects of fuel cells: a review. Sci Total Environ 2021/01/15/2021;752:141803. https://doi.org/10.1016/j.scitotenv.2020.141803.
[8] Luo Y, Wu Y, Li B, Qu J, Feng SP, Chu PK. Optimization and cutting-edge design of fuel-cell hybrid electric vehicles. Int J Energy Res 2021;45(13):18392–423.
[9] Fan L, Tu Z, Chan SH. Recent development of hydrogen and fuel cell technologies: a review. Energy Rep 2021/11/01/2021;7:8421–46. https://doi.org/10.1016/j.egyr.2021.08.003.

[10] Bargal MHS, Abdelkareem MAA, Tao Q, Li J, Shi J, Wang Y. Liquid cooling techniques in proton exchange membrane fuel cell stacks: a detailed survey. Alex Eng J 2020/04/01/2020;59(2):635–55. https://doi.org/10.1016/j.aej.2020.02.005.

[11] Hua M, Chen G, Zhang B, Huang Y. A hierarchical energy efficiency optimization control strategy for distributed drive electric vehicles. Proc Inst Mech Eng - Part D J Automob Eng 2019;233(3):605–21. https://doi.org/10.1177/0954407017751788.

[12] Chengqing Wen JL, Zhou Quan, Lu Guoxiang, Xu Hongming. Thermal efficiency predictive modelling of dedicated hybrid engines based on an optimal multi-network structure. Int J Powertrains 2023. https://doi.org/10.1504/IJPT.2024.10056926.

[13] Pili R, García Martínez L, Wieland C, Spliethoff H. Techno-economic potential of waste heat recovery from German energy-intensive industry with Organic Rankine Cycle technology. Renew Sustain Energy Rev 2020/12/01/2020;134:110324. https://doi.org/10.1016/j.rser.2020.110324.

[14] Hussain A, Arif SM, Aslam M. Emerging renewable and sustainable energy technologies: state of the art. Renew Sustain Energy Rev 2017/05/01/2017;71:12–28. https://doi.org/10.1016/j.rser.2016.12.033.

[15] Ngwaka U, Chen F, Qiu S, Li M, Zhang C, Wu D. Recent progress on performance and control of linear engine generator. Int J Engine Res 2022. https://doi.org/10.1177/1468087422111801.

[16] Mikalsen R, Roskilly AP. A review of free-piston engine history and applications. Appl Therm Eng Oct 2007;27(14–15):2339–52. https://doi.org/10.1016/j.applthermaleng.2007.03.015 (in English).

[17] Wang Y, Chen L, Jia B, Roskilly AP. Experimental study of the operation characteristics of an air-driven free-piston linear expander. Appl Energy 2017;195:93–9. https://doi.org/10.1016/j.apenergy.2017.03.032.

[18] Li M, Ngwaka U, Moeini Korbekandi R, Baker N, Wu D, Tsolakis A. A closed-loop linear engine generator using inert gases: a performance and exergy study. Energy 2023/10/15/2023;281:128278. https://doi.org/10.1016/j.energy.2023.128278.

[19] Zhang F, Chen G, Wu D, Li T, Zhang Z, Wang N. Characterising premixed ammonia and hydrogen combustion for a novel Linear Joule Engine Generator. Int J Hydrogen Energy 2021;46(44):23075–90. https://doi.org/10.1016/j.ijhydene.2021.04.110.

[20] Ngwaka U, et al. Parametric analysis of a semi-closed-loop linear joule engine generator using argon and oxy-hydrogen combustion. Energy 2021/02/15/2021;217:119357. https://doi.org/10.1016/j.energy.2020.119357.

[21] Zhou Y, Sofianopoulos A, Lawler B, Mamalis S. Advanced combustion free-piston engines: a comprehensive review. Int J Engine Res 2020;21(7):1205–30. https://doi.org/10.1177/1468087418800612.

[22] Van Blarigan P, Paradiso N, Goldsborough S. Homogeneous charge compression ignition with a free piston: a new approach to ideal Otto cycle performance. SAE Technical Paper 1998;982484. https://doi.org/10.4271/982484.

[23] Clark NN, et al. Modeling and development of a linear engine. In: Presented at the spring technical conference, ASME ICE division; 1998. Fort Lauderdale, FL.

[24] Jia B, Tian G, Feng H, Zuo Z, Roskilly A. An experimental investigation into the starting process of free-piston engine generator. Appl Energy 2015;157:798–804. https://doi.org/10.1016/j.apenergy.2015.02.065.

[25] Jia B, Zuo Z, Tian G, Feng H, Roskilly AP. Development and validation of a free-piston engine generator numerical model. Energy Convers Manag 2015;91:333–41. https://doi.org/10.1016/j.enconman.2014.11.054.

[26] Lu J, Xu Z, Liu L. Compression ratio control of an opposed-piston free-piston engine generator based on artificial neural networks. IEEE Access 2020;8:107865–75. https://doi.org/10.1109/ACCESS.2020.3001273.

[27] Mikalsen R, Roskilly AP. The free-piston reciprocating Joule Cycle engine: a new approach to efficient domestic CHP generation. In: Proceeding of ICAE2012 conference. Citeseer; 2012.

[28] Jia B, Wu D, Smallbone A, Lawrence C, Roskilly AP. Design, modelling and validation of a linear Joule Engine generator designed for renewable energy sources. Energy Convers Manag 2018;165:25–34. https://doi.org/10.1016/j.enconman.2018.03.050.

[29] Jia B, Wu D, Smallbone A, Ngwaka UC, Roskilly AP. Dynamic and thermodynamic characteristics of a linear Joule engine generator with different operating conditions. Energy Convers Manag 2018;173:375–82. https://doi.org/10.1016/j.enconman.2018.07.098.

[30] P. Team. "When is a Standard Pneumatic Valve Not Good Enough?" https://blog.parker.com/site/usa/details-home-page/when-is-a-standard-pneumatic-valve-not-good-enough-us (accessed)..

[31] Venkataraman K, Kanthavel K, Kumar BN. Investigations of response time parameters of a pneumatic 3/2 direct acting solenoid valve under various working pressure conditions. Eng Technol Appl Sci Res 2013;3(4):502–5. https://doi.org/10.48084/etasr.360.

[32] A. M. Sada-Regalado, D. F. Novella-Rodriguez, and J. C. Tudon-Martínez, "Simulation and analysis of the actuation system in a camless piston engine."..

[33] Lou Z, Zhu G. Review of advancement in variable valve actuation of internal combustion engines. Appl Sci 2020;10(4):1216. https://doi.org/10.3390/app10041216.

[34] Sun M, et al. Progress in camless variable valve actuation with two-spring pendulum and electrohydraulic latching. SAE International Journal of Engines 2013;6(1):319–26. https://doi.org/10.4271/2013-01-0590.

[35] Ma J, Zhu GG, Schock H. A dynamic model of an electropneumatic valve actuator for internal combustion engines. J Dyn Syst Meas Control 2010;132(2). https://doi.org/10.1115/1.4000816.

[36] Ma J, Zhu GG, Schock H. Adaptive control of a pneumatic valve actuator for an internal combustion engine. IEEE Trans Control Syst Technol 2010;19(4):730–43. https://doi.org/10.1109/ACC.2007.4282267.

[37] Wu S, Jiao Z, Yan L, Zhang R, Yu J, Chen C-Y. Development of a direct-drive servo valve with high-frequency voice coil motor and advanced digital controller. IEEE ASME Trans Mechatron 2013;19(3):932–42. https://doi.org/10.1109/TMECH.2013.2264218.

[38] Khandaker MF, Hong H, Rodrigues L. Modeling and controller design for a voice coil actuated engine valve. In: Proceedings of 2005 IEEE conference on control applications, 2005. IEEE; 2005. p. 1234–9. https://doi.org/10.1109/CCA.2005.1507300. *CCA 2005*.

[39] Liu L, Chang S. Motion control of an electromagnetic valve actuator based on the inverse system method. Proc Inst Mech Eng - Part D J Automob Eng 2012;226:85–93. https://doi.org/10.1177/0954407011413033.

[40] Fan X, Yin J, Lu Q. Design and analysis of a novel composited electromagnetic linear actuator. Actuators 2021;11(1):6. https://doi.org/10.3390/act11010006. MDPI.

[41] X. Fan, J. Yin, and Q. Lu, "Design and analysis of a novel composited electromagnetic linear actuator," Actuators, vol. 11, no. 1, doi: 10.3390/act11010006..

[42] Watson JP, Wakeman RJ. Simulation of a pneumatic valve actuation system for internal combustion engine. SAE technical paper, 0148-7191. 2005.

[43] Shao D, Sichuan X, Du A. Research on a new electromagnetic valve actuator based on voice coil motor for automobile engines. SAE technical paper, 0148-7191. 2017.

[44] Li B, Gao L, Yang G. Modeling and control of a novel high-pressure pneumatic servo valve direct-driven by voice coil motor. J Dyn Syst Meas Control 2013;135(1):014507. https://doi.org/10.1115/1.4007702.

[45] Qiao Y, Zhao T, Gui X. Overview of position servo control technology and development of voice coil motor. CES Transactions on Electrical Machines and Systems 2022;6(3):269–78. https://doi.org/10.30941/CESTEMS.2022.00037.

[46] Chai J, Gui X. Overview of structure optimization and application of voice coil motor. Trans China Electrotech Soc 2021;36:1114–25. https://doi.org/10.19595/j.cnki.1000-6753.tces.200725.

[47] Shiao Y, Kantipudi MB, Weng C-B. New actuation control for hybrid electromagnetic valve train. Appl Sci 2022;12(20):10449.

[48] Li M, Ngwaka U, Wu D, Zhang F, Chen G. The design and simulation of the linear engine generator used for electric propulsion system of the marine transportation and offshore gas/oil platforms. In: Presented at the 7th international conference on ship and offshore technology ICSOT Surabaya, Indonesia; 2021. November 2021.

[49] Ngwaka U, Jia B, Lawrence C, Wu D, Smallbone A, Roskilly AP. The characteristics of a Linear Joule Engine Generator operating on a dry friction principle. Appl Energy 2019;237:49–59. https://doi.org/10.1016/j.apenergy.2018.12.081.

[50] R. Moeini Korbekandi, N. J. Baker, M. C. Kulan, A. S. Jalal, D. Wu, and M. Li, "Dynamic characteristics and demonstration of an integrated linear engine generator with alternative electrical machines," Energies, vol. 15, no. 14, doi: 10.3390/en15145295..

[51] Perry Jr J. Critical flow through sharp-edged orifices. Trans Am Soc Mech Eng 1949;71(7):757–63. https://doi.org/10.1115/1.4017216.

[52] McCloy D, Martin HR. Control of fluid power: analysis and design. Chichester, Sussex, England: Halsted Press; 1980. p. 505. Ellis Horwood, Ltd.; New York.

[53] Hsu C-F, Chen B-R, Wu B-F. Fuzzy broad learning adaptive control for voice coil motor drivers. Int J Fuzzy Syst 2022:1–12. https://doi.org/10.1007/s40815-021-01227-2.

[54] Batts Z, Kim J, Yamane K. Design of a hopping mechanism using a voice coil actuator: linear elastic actuator in parallel (LEAP). In: 2016 IEEE international conference on robotics and automation (ICRA). IEEE; 2016. p. 655–60. https://doi.org/10.1109/ICRA.2016.7487191.

[55] Stefański A, Wojewoda J, Wiercigroch M, Kapitaniak T. Chaos caused by non-reversible dry friction. Chaos, Solit Fractals 2003/06/01/2003;16(5):661–4. https://doi.org/10.1016/S0960-0779(02)00451-4.

[56] Stranton JF, Taylor JC. Friction coefficients for stainless steel (PTFE) Teflon bearings. Madison, WI: Wisconsin Highway Research Program; 2010.

[57] Watkins WH. Back EMF. In: Watkins WH, editor. Loudspeaker physics and forced vibration. Cham: Springer International Publishing; 2022. p. 37–43.

[58] Schechter MM, Levin MB. Camless engine. SAE technical paper, 0148-7191. 1996.

[59] Picron V, Postel Y, Nicot E, Durrieu D. Electro-magnetic valve actuation system: first steps toward mass production. SAE technical paper, 0148-7191. 2008.

[60] Tang Y, He Y, Wang F, Lee DH, Ahn JW, Kennel R. Back-EMF-based sensorless control system of hybrid SRM for high-speed operation. IET Electr Power Appl 2018;12(6):867–73. https://doi.org/10.1049/iet-epa.2017.0641.

[61] Okada Y, Marumo Y, Konno M. Electromagnetic valve actuator for automobile engines. SAE Technical Paper 2004-01-1387; 2004.

[62] Lou ZD, et al. Progress in camless variable valve actuation with two-spring pendulum and electrohydraulic latching. SAE International Journal of Engines 2013;6(1):319–26.

[63] Theobald MA, Lequesne B, Henry R. Control of engine load via electromagnetic valve actuators. SAE Trans 1994:1323–34.

[64] Pan J, Khajepour A, Li Y, Yang J, Liu W. Performance and power consumption optimization of a hydraulic variable valve actuation system. Mechatronics 2021;73:102479.

[65] Xu J, Chang S, Fan X, Fan A. Effects of electromagnetic intake valve train on gasoline engine intake charging. Appl Therm Eng 2016/03/05/2016;96:708–15. https://doi.org/10.1016/j.applthermaleng.2015.10.163.